Microscopic study of structure of light- and medium-mass even-even cadmium isotopes

Shivali Sharma, Rani Devi,* and S. K. Khosa
Department of Physics, University of Jammu, Jammu, Jammu and Kashmir-180006, India

(Received 2 November 2020; revised 5 April 2021; accepted 1 June 2021; published 14 June 2021)

The potential-energy surfaces (PESs) for ground states of even-even $^{102-112}$Cd isotopes are obtained by using the three-dimensional relativistic Hartree-Bogoliubov model with the density-dependent meson exchange interaction. The quadrupole deformation parameters are extracted from the PES calculations and employed in the beyond mean-field projected shell model to study the yrast and excited states of these isotopes. Besides, the $E2$ transition probabilities and g factors are obtained and compared with the experimental data. The present calculations support the experimental finding that yrast 8^+ states of light Cd isotopes are of $(\pi g_{9/2})^2$ character whereas the yrast 10^+ states of medium-mass Cd isotopes are found to possess $(\nu h_{11/2})^2$ character.

DOI: 10.1103/PhysRevC.103.064312

I. INTRODUCTION

The cadmium (Cd) isotopes are nuclei having atomic number $(Z) = 48$ and fall very close to nuclei characterized by $Z = 50$ shell closure for protons. The low-lying excitation energy spectra of these nuclei exhibit a typical vibrational nature with onset of moderate deformation at higher spins. This dilemma of having low-lying vibrational spectra up to certain spins and the onset of quasirotational character at higher spins has been the subject of study over the past a few decades for Cd isotopes. One finds that intensive experimental [1–23] and theoretical [24–29] attempts have been made to elucidate the structure of Cd isotopes. The experimental effort is mainly directed at determining the excitation energy spectra, lifetimes of nuclear excited states, $B(E2)$ transition probability values, and g factors. A lucid overview of literature on this is presented hereunder.

The energy spectra of these Cd isotopes have been obtained using various experimental techniques. De Angelis *et al.* [1] determined the high spin structure of ^{104}Cd and extended the previously identified level scheme up to an excitation energy of 11.9 MeV. Kumpulainen *et al.* [2] used the in-beam and off-beam γ-ray and conversion electron spectroscopy to study the low spin states in $^{106-112}$Cd. Juutinen *et al.* [3] extended the yrast band to high spins and obtained some side bands in ^{110}Cd. Corminboeuf *et al.* [4] added one new 2^+ level at an energy of 3042.841 keV to the already observed level scheme of ^{110}Cd and found ten new transitions. They have also obtained the lifetimes of 16 states in ^{110}Cd. The lifetimes of various nuclear excited states have been measured by various experimental groups. These lifetime measurements are used to compute the $B(E2)$ transition rates. Lieb *et al.* [5] for the first time measured the lifetime of excited states above spin $I = 10^+$ in ^{102}Cd and deduced the reduced transition strengths from the lifetimes. Boelaert *et al.* [6] in their paper focused on the low spin states of ^{102,104}Cd and measured the lifetimes of 2^+ and 4^+ states in ^{104}Cd and the first 2^+ state in ^{102}Cd by employing the recoil distance Doppler-shift (RDDS) technique. Muller *et al.* [7] employed the RDDS technique and for the first time determined the lifetimes of high spin states in ^{104}Cd. They have also deduced $B(E2)$ values of the high spin states and discussed the new experimental results in the framework of interacting boson plus broken pair model. Simons *et al.* [8] measured the lifetimes of excited states in ^{106,108}Cd and deduced the $B(E2)$ values for corresponding spin states. Benczer-Koller *et al.* [9] remeasured the lifetimes and magnetic moments of excited states in ^{106}Cd. Piiparinen *et al.* [10] determined the lifetimes of many yrast levels in ^{110}Cd and deduced $B(E2)$ values from them. Harissopulos *et al.* [11] measured the mean lifetime of the lowest six yrast band members and nine excited states in ^{110}Cd and ^{109}Cd, respectively, by the RDDS technique. Garrett *et al.* [12] measured the lifetimes of levels below 4 MeV in ^{112}Cd by using Doppler-shift attenuation technique, and transition rates have been deduced for γ-ray decays. In their subsequent work [13], they performed more precise measurement of the lifetimes and extracted more precise $B(E2)$ values for various states of ^{110}Cd. The coexistence of shapes in ^{110,112}Cd has also been reported in their recent studies [14,15].

On the theoretical side, the shell model [24,25], the interacting boson model [26], the microscopic time-dependent Hartree-Fock-Bogoliubov [27], the Skyrme density functional [28], and the generalized seniority scheme [29] studies have been carried out for some Cd isotopes.

Despite extensive experimental studies, the individual theoretical models have not been able to establish a clear picture of the structure of these even-even Cd isotopes. The light Cd isotopes with two proton holes and a few neutrons above $N = 50$ are found to exhibit vibrational character at low spins. The medium-mass Cd with $A = 106$–112 is observed to exhibit weakly deformed structures. The magnetic moment measurements reveal that the yrast 8^+ states of light Cd isotopes [16] are of pure $(\pi g_{9/2})^2$ character whereas the yrast 10^+ states

*Corresponding author: rani_rakwal@yahoo.co.in

of medium-mass Cd isotopes [18,21,23] are found to possess $(\nu h_{11/2})^2$ character. Besides this, the measurement of g factors has also become possible for some of the nuclear excited states in some Cd isotopes. Alber *et al.* [16] measured the g factor of the 8^+ state as 1.29(3) by using the perturbed angular momentum distribution (PAD) method. The g factor of this state was predicted to be of almost pure proton structure. They observed a considerable quenching in the value of $g(8_1^+)$ of ^{102}Cd in comparison to the $g(8_1^+)$ of semimagic $N = 50$ ^{96}Pd due to neutron excitations. Wang *et al.* [17] measured the g factor as 0.28 ± 0.05 of the 2_1^+ state in ^{110}Cd. Regan *et al.* [18] measured the value of the g factor of the 10^+ state in ^{110}Cd as $-0.09(3)$ by using the ion-implantation PAD technique. This value was smaller than expected for a pure two-neutron $(h_{11/2})^2$ configuration. The difference was attributed to the mixing of collective and (or) proton components in the wave function in the 10^+ state. Brennan *et al.* [19] measured the $g(2_1^+)$ of $^{106-116}$Cd by using the dynamic-field technique and compared the experimental data with the vibrational and interacting boson models. The g factor of the 4_1^+ state in ^{106}Cd was measured for the first time by Kumbartzki *et al.* [20] by using the transient field technique. Fan *et al.* [21] measured the g factors of states above the $I = 8^+$ spin in ^{108}Cd by using the transient magnetic-field ion-implantation PAD method. The g factors of some of the Cd isotopes have also been remeasured recently [9,22,23]. Chamoli *et al.* [22] remeasured the g factors of the 2_1^+ states in Cd isotopes and compared them with the tidal wave version of the cranking model. They evaluated the spin contributions to single-particle magnetic moments by taking an attenuation factor of 0.70. They proposed that the more accurate predictions of g factors are required by including pairing self-consistently in the model. Benczer-Koller *et al.* [9] remeasured the values of the $g(2_1^+)$ and $g(4_1^+)$ in ^{106}Cd and found the measured value of $g(4_1^+)$ to be only 59% of $g(2_1^+)$. The shell-model and tidal wave model [22] calculations could not reproduce the g factor of the 4_1^+ state. However, shell-model calculations with an effective nucleon g factor yielded $g(4_1^+) < g(2_1^+)$ but under predicted the $g(2_1^+)$ value. Gray *et al.* [23] remeasured the value of the g factor of the 10^+ state to be $-0.29(16)$ in ^{110}Cd by using time-differential PAD technique. They confirmed the $(\nu h_{11/2})^2$ configuration for the 10^+ state by quenching the Schmidt value of the g factor of -0.348 for this configuration by 70% of the free nucleon value to -0.243. Based on the availability of extensive experimental data on even-even light- and medium-mass Cd isotopes the following striking features are observed in these isotopes:

(i) Evolution of the ground-state shape as a function of A.
(ii) The existence of multiple 6^+, 8^+, and 10^+ states in the excitation energy spectra.
(iii) Depletion in the magnitude of $B(E2)$ transition probabilities at specific spins.
(iv) Onset of weak deformation at $I = 8^+$ and 10^+ states in light- and medium-mass Cd isotopes.

In order to elucidate the above features, the ground states as well as the excited states of light- and medium-mass even-even Cd isotopes are studied by employing relativistic and beyond mean-field approaches. To establish the ground-state shapes of these isotopes three-dimensional relativistic Hartree-Bogoliubov (RHB) model [30,31] with the density-dependent meson exchange (DD-ME2) [32] interaction is employed. Subsequently, the quadrupole deformation parameters (β_2) extracted from the potential-energy surface (PES) calculations of these isotopes are fed as input quadrupole deformation parameters ($\epsilon_2 \approx 0.95\beta_2$) in the projected shell model (PSM) to study the structure of excited states. The resulting wave functions are then used to calculate the electromagnetic quantities which are sensitive quantities employed to check the reliability and validity of the theoretical models. The organization of the paper is as follows: In Sec. II, a brief outline of the theoretical models is presented. In Sec. III, the results of PES are discussed. Section IV presents the PSM results on excited states. In Sec. V, a summary of the conclusions drawn from the presented paper are listed.

II. THEORETICAL FRAMEWORKS

The theoretical frameworks used to study the even-even $^{102-112}$Cd isotopes are briefly outlined in this section.

In the first step, the self-consistent triaxial RHB calculations are carried out for each Cd isotope to obtain the PESs in the (β, γ) quadrupole space. The PESs for even-even $^{102-112}$Cd have been obtained by using the triaxial RHB method with the separable pairing model [33]. For the details of the triaxial RHB model, the reader is referred to Refs. [30,31]. The DD-ME2 interaction [32] is used to perform RHB calculations. The numerical details of the calculation are as follows: Twelve major oscillator shells for fermions and 20 major oscillator shells for bosons are taken into account for the basis in the present calculations. The PESs of even-even $^{102-112}$Cd isotopes have been obtained by imposing constraints on the mass quadrupole moments of axial and triaxial deformation parameters.

The method of quadratic constraint employs an unrestricted variation of the function,

$$\langle \hat{H} \rangle + \sum_{\mu=0,2} C_{2\mu}(\langle \hat{Q}_{2\mu} \rangle - q_{2\mu})^2, \tag{1}$$

where $\langle \hat{H} \rangle$ and $\langle \hat{Q}_{2\mu} \rangle$ are total energy and expectation value of mass quadrupole operators ($\hat{Q}_{20} = 2z^2 - x^2 - y^2$ and $\hat{Q}_{22} = x^2 - y^2$), respectively. The constrained value of the multipole moment is represented by $q_{2\mu}$, and the corresponding stiffness constant is represented by $C_{2\mu}$. For the self-consistent solution, the extra force term $\sum_{\mu=0,2} \lambda_\mu \hat{Q}_{2\mu}$ is added to the system by the quadratic constraint, here $\lambda_\mu = 2C_{2\mu}(\langle \hat{Q}_{2\mu} \rangle - q_{2\mu})$. This term is essential for putting the system to a point in deformation space different from the stationary point.

The PESs of even-even $^{102-112}$Cd, obtained from the above-mentioned triaxial RHB calculations are displayed in Fig. 1. At least, one prolate minimum with moderate deformation is found in all the considered Cd isotopes. In the case of ^{108}Cd, the calculations predict coexistence of two prolate minima at different deformations. However, in the case of ^{110,112}Cd one prolate and one triaxial minima are predicted. Experimentally,

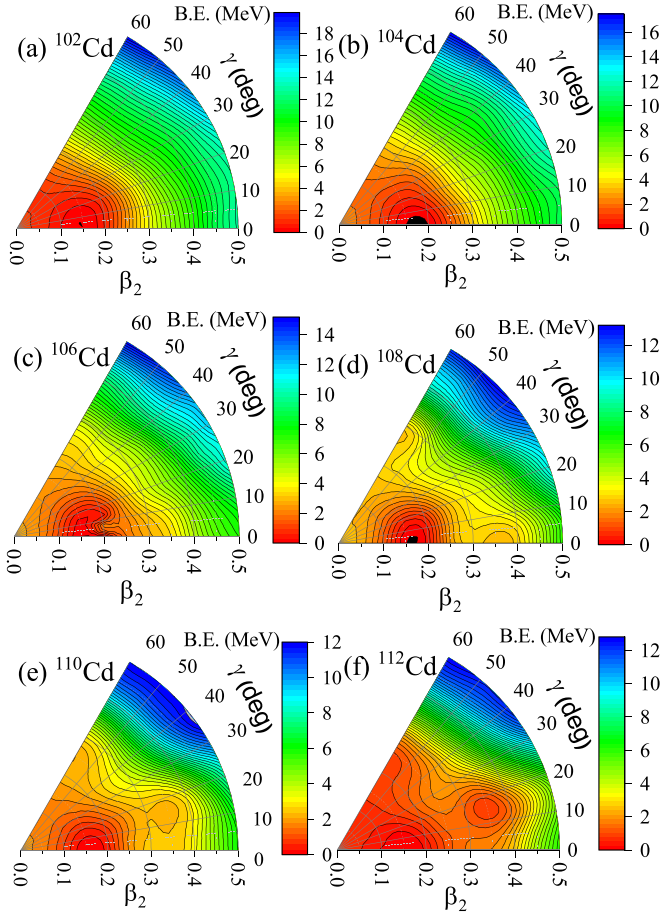

FIG. 1. PES of the even-even $^{102-112}$Cd isotopes, that have been obtained with the relativistic Hartree-Bogoliubov model on the β-γ plane ($0 \leqslant \gamma \leqslant 60^{\circ}$) with the DD-ME2 interaction. All energies are normalized with respect to the binding energy of the absolute minima. The color bar refers to the energy of each point on the surface relative to the minimum.

Garrett *et al.* [14,15] have also reported the coexistence of shapes in ^{110,112}Cd. The values of quadrupole deformation parameter (β_2) are extracted from these PESs and are presented in Table I. The values of β_2 extracted from the PESs are converted to ϵ_2 by using the relation $\epsilon_2 \approx 3/2(5/4\pi)^{1/2}\beta_2$. These values of ϵ_2 are used as input for carrying out PSM calculations.

In the next step, the values of ϵ_2 obtained from the RHB calculation are taken as input deformation parameters in PSM to study the excited-state properties of $^{102-112}$Cd. The PSM has been employed to study the excitation spectra and electromagnetic quantities of $^{102-112}$Cd isotopes. PSM is a shell model built over the deformed basis which incorporates pairing through the Bardeen-Cooper-Schrieffer (BCS) calculation. For details of the PSM framework, the reader is referred to Refs. [34–36]. The brief outline of the working of this model is as follows:

TABLE I. The values of quadrupole deformation parameter (β_2), extracted from the PES and the proportionality constant η.

Nuclei	^{102}Cd	^{104}Cd	^{106}Cd	^{108}Cd	^{110}Cd	^{112}Cd
β_2	0.14	0.17	0.15	0.16	0.18	0.15
η	0.26	0.22	0.19	0.19	0.18	0.19

First, the Nilsson Hamiltonian is diagonalized for the known deformation parameter ϵ_2 which provides the deformed single-particle states. The monopole pairing force is incorporated into these states by a BCS calculation. The Nilsson + BCS calculation defines the deformed quasiparticle (qp) basis in the PSM. The truncation of the configuration space within the deformed mean field is performed by selecting only the BCS vacuum and few qp configurations in the Nilsson orbitals around the Fermi surface. Here for the present study of Cd isotopes three major harmonic-oscillator shells $N = 2$–4 for protons and $N = 3$–5 for neutrons are considered. The qp basis is constructed from the last harmonic-oscillator shells. The Nilsson parameters are taken from Ref. [37].

The multi-qp states considered in the present calculations are as

$$|\phi_\kappa\rangle = \{|0\rangle, a_\nu^\dagger a_\nu^\dagger|0\rangle, a_\pi^\dagger a_\pi^\dagger|0\rangle, a_\nu^\dagger a_\nu^\dagger a_\pi^\dagger a_\pi^\dagger|0\rangle\}, \quad (2)$$

where $|0\rangle$ is the Nilsson-BCS qp vacuum (at a deformation ϵ_2) where all neutrons and protons are paired, giving the lowest energy with zero spin and positive parity. The $a_\nu^\dagger a_\nu^\dagger|0\rangle, a_\pi^\dagger a_\pi^\dagger|0\rangle$ and $a_\nu^\dagger a_\nu^\dagger a_\pi^\dagger a_\pi^\dagger|0\rangle$ are excited two quasi-neutron, excited two quasi-proton, and low-lying 4-qp (two quasi-neutron $\otimes$ two quasi-proton) configurations, respectively.

The axial symmetry is assumed in the present calculations, and the angular momentum projection technique [38] is applied on the chosen Nilsson + BCS quasiparticle states to form shell-model configurations in the laboratory frame. The Hamiltonian chosen in the PSM is a sum of the spherical single-particle Hamiltonian, quadrupole-quadrupole (Q,Q) plus monopole and quadrupole pairing forces. The strength of the Q,Q force is determined in a self-consistent manner so that it generates the correct nuclear deformation of the basis [34]. The monopole-pairing strength for neutrons (G_M^ν) and protons (G_M^π) is of the form

$$G_M^\nu = \left[G_1 - G_2\frac{N-Z}{A}\right]A^{-1}(\text{MeV}),$$
$$G_M^\pi = G_1 A^{-1}(\text{MeV}).$$

The value of constants G_1 and G_2 are taken as 19.60 and 15.70, which are damped by factors of 0.95 and 1.25, respectively, for reproducing the known pairing gaps in the mass region under study. The quadrupole pairing strength G_Q is proportional to G_M with the proportionality constant η, and the values taken for it are listed in Table I.

Finally, the shell-model Hamiltonian is diagonalized within the shell-model space spanned by the selected set of projected multi-qp states of Eq. (2). As a result of the diagonalization of the Hamiltonian, a set of eigenstates is obtained for a given spin. The energy corresponding to each lowest spin gives the measure of yrast energy. In addition to yrast states, a number of excited states are also obtained for the

nucleus under study. The yrast and excited states obtained after configuration mixing are compared with the available experimental data. In order to test the resulting PSM wave functions, the electromagnetic quantities are calculated and compared with the experimental data.

III. PES

In Fig. 1, the PES plots are drawn for $^{102-112}$Cd, obtained from the RHB calculations mentioned in Sec. II. Figure 1 depicts all the considered Cd isotopes to have prolate minimum with moderate axial deformation of $\cong$ 0.15–0.18. Thus, three-dimensional RHB calculations establish that $^{102-112}$Cd are prolate moderate axial deformed isotopes in their ground states. In order to study the excited-state properties of these isotopes beyond the mean-field approach, PSM is applied. The excitation spectra are obtained by using the axial PSM approach, and the resulting PSM wave functions are used to compute the $E2$ transition probabilities and g factors of the considered Cd isotopes. In the RHB model the potential-energy minima are obtained. By taking this input deformation PSM calculations are carried out where the pairing interaction is used for the quasiparticles in the deformed basis. It is known that pairing plays an important role in determining the ground-state properties and low-lying excitation energy spectra in the open-shell nuclei studied in the present paper. Therefore, the type of pairing employed in the RHB and PSM calculations in the present paper should have been the same. Since the pairing interaction used in the RHB and PSM models are not of the same type, there arises some inconsistency in the use of the pairing interaction. To minimize the effect of such inconsistency, the deformation parameters obtained from RHB calculation have been used as input deformation for carrying out the PSM calculation with the caution that the strength of the quadrupole-quadrupole two-body interaction in the PSM model is varied in a self-consistent manner so that it generates the same nuclear deformation of the basis as was produced by RHB calculations for the ground state. To check further on the issue of inconsistency in the implementation of the pairing interaction, the change in the energy spectra has been calculated by varying the pairing parameter η. It turns out that these changes are very small when η is varied around the stable value listed in Table I for each nucleus. For example, in ^{104}Cd the percentage change in E_{2^+} is 9.7, and for E_{14^+} the percentage change is 1.5 when the percentage change in pairing parameter η is 9.1. In addition, we have also calculated the pairing gaps for neutrons at the Fermi level arising from PSM and RHB calculations for each nucleus and found them to be comparable. The calculated values of pairing gaps are given in Table II. From the nature of the agreement for the pairing gaps and small values of percentage change in energy spectra, the calculational results presented in this paper are reasonably stable.

IV. COMPARISON OF THEORETICAL RESULTS WITH EXPERIMENTAL DATA

The theoretical results obtained for excitation spectra and electromagnetic quantities in the framework of the PSM are compared with the experimental data in the following subsections.

TABLE II. The calculated values of pairing gaps for neutrons from PSM and RHB calculations.

Nuclei	^{102}Cd	^{104}Cd	^{106}Cd	^{108}Cd	^{110}Cd	^{112}Cd
PSM	0.844	0.888	0.937	0.992	1.008	0.990
RHB	0.789	0.791	0.926	0.869	0.943	1.204

A. Excitation spectra

The yrast and excited energy states are obtained after configuration mixing and shell-model diagonalization. The comparison of theoretical and experimental excitation spectra is presented in the following subsections:

1. Yrast states

In Fig. 2, the comparison of the theoretical and experimental excitation spectra is presented for $^{102-112}$Cd. The experimental data are taken from Refs. [5,7,39–42]. The predicted configurations of the yrast state are presented in Tables I and II of the Supplemental Material [43]. In all the considered Cd isotopes, the yrast energies up to $I = 4^+$ reproduce well the experimental data and arise from pure ground-state (0-qp) configuration. The predicted yrast 6^+ and 8^+ states have 75% admixtures of two quasiparticle (2-qp) $(\pi g_{9/2})^2$ configuration in addition to a 0-qp configuration in all the considered Cd isotopes. The predicted yrast 10^+ states in ^{102,104}Cd [Figs. 2(a) and 2(b)] have the same character as the 6^+ and 8^+ states but the character of the yrast 10^+ states changes in $^{106-112}$Cd [Figs. 2(c)–2(f)] to 2-qp $(\nu h_{11/2})^2$. The probabilities of the 2-qp $(\nu h_{11/2})^2$ configuration in $^{106-112}$Cd are 95.7%, 97.4%, 98.6%, and 98.3%, respectively. The yrast 12^+ states in $^{106-112}$Cd arise from the 2-qp $(\nu h_{11/2})^2$ configuration with 90.4%, 92.5%, 93.6%, and 92.3% probabilities, respectively. The yrast 14^+ state in ^{102}Cd and the 12^+ state in ^{104}Cd arise from the 2-qp $(\nu h_{11/2})^2$ configuration with 89% and 79.8% probabilities, respectively. The yrast 14^+ states in $^{104-112}$Cd arise from an admixture of 2-qp $(\nu h_{11/2})^2$ and 4-qp $(\nu h_{11/2} \otimes \pi g_{9/2})$ configurations. The probabilities of the neutron 2-qp and 4-qp configurations in the 14^+ state of $^{104-112}$Cd are 85.7%, 9.8%, 82.2%, 15.9%, 75%, 21.4%, 68.5%, 28.7%, 65.2%, and 31.3%, respectively. In the case of ^{112}Cd, the yrast 6^+ state has an admixture of 0-qp, 2-qp $(\pi g_{9/2})^2$ and $(\nu h_{11/2})^2$ configurations with 64.5%, 11.5%, and 19.8% probabilities, respectively, whereas the 8^+ to 12^+ states have 2-qp $(\nu h_{11/2})^2$ as the dominant configuration with 98.8%, 97.3%, and 91.6% probabilities, respectively. The higher spin yrast states in $^{106-112}$Cd are underestimated as the measurement of some of the observed energies may be tentative. The experimental excitation energies in ^{104}Cd have been revised by Muller *et al.* [7] which are well reproduced by the present calculations. The configuration of the yrast 10^+ states changes from $(\pi g_{9/2})^2$ to $(\nu h_{11/2})^2$ as one moves from ^{106}Cd to ^{108}Cd. Thus, the yrast 10^+ states in light

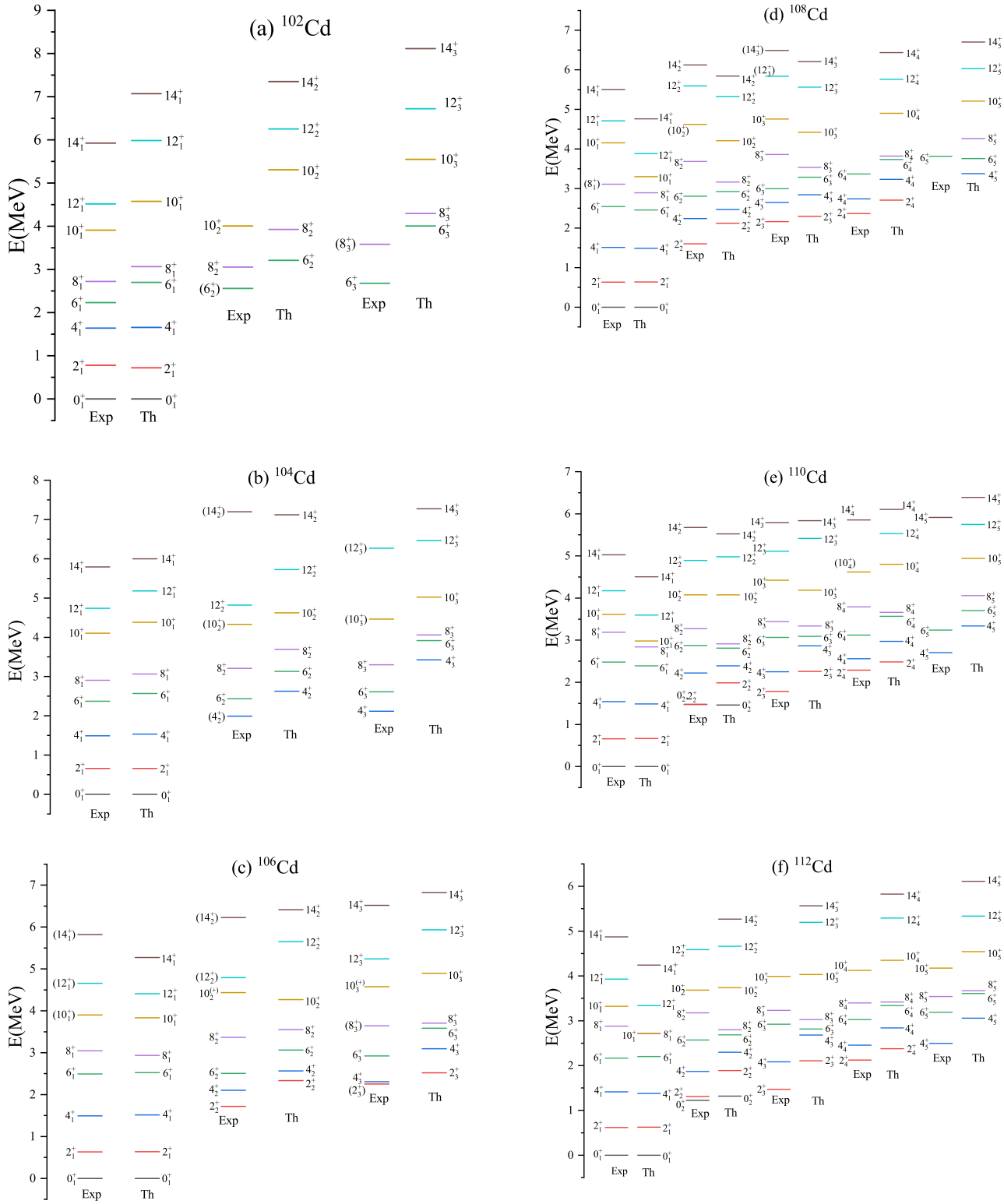

FIG. 2. Comparison of calculated (Th) energy states with available experimental (Exp) data for (a) ^{102}Cd [5], (b) ^{104}Cd [7], (c) ^{106}Cd [39], (d) ^{108}Cd [40], (e)^{110}Cd [41], and (f) ^{112}Cd [15,42].

^{102,104}Cd arise from the 2-qp $(\pi g_{9/2})^2$ configuration whereas in $^{106-112}$Cd the yrast 10^+ states arise from the 2-qp $(\nu h_{11/2})^2$ configuration in accordance with the experimental observation [16,18,21,23].

2. *Excited states*

The predicted configurations of excited states in $^{102-112}$Cd are presented in Tables I and II of the Supplemental Material [43]. The excited states in some of the considered Cd

TABLE III. Comparison of experimental [5–7,9–13,39–42,46–49] and theoretical $B(E2)$ values (in units of e^2b^2). The theoretical values are given in bold in the last row corresponding to each transition.

Transition	^{102}Cd	^{104}Cd	^{106}Cd	^{108}Cd	^{110}Cd	^{112}Cd
$2_1^+ \to 0_1^+$	0.0562(90)[a]	0.0779(27)[a]	0.0852(34)[d]	0.0884(36)[d]	0.0934(38)[d]	0.1048(42)[d]
	>0.0354[b]	0.0735($^{+365}_{-184}$)[c]	0.0749(44)[e]	0.0813(9)[h]	0.0894(70)[j]	0.0971(6)[o]
			0.115(8)[f]		0.0848(250)[k]	
					0.0751(94)[l]	
					0.0720(5)[m]	
	0.0634	**0.0746**	**0.0847**	**0.0893**	**0.0935**	**0.0969**
$4_1^+ \to 2_1^+$	>0.0225[b]	0.1352(488)[a]	0.1336(93)[e]	0.1252(183)[h]	0.1315(219)[k]	0.2020(256)[o]
		>0.0336[c]	0.069(4)[f]		0.1503(751)[l]	0.1956(192)[p]
					0.1440(187)[m]	
	0.1042	**0.1191**	**0.1324**	**0.1418**	**0.1494**	**0.1565**
$4_2^+ \to 2_1^+$					0.0004(2)[n]	
					0.0006($^{+2}_{-3}$)[k]	
		0.0009	**0.0028**	**0.0016**	**0.0006**	**0.000037**
$4_2^+ \to 2_2^+$					0.0689(313)[n]	
					0.1002($^{+313}_{-438}$)[k]	
	0.0535	**0.0668**	**0.0703**	**0.0378**	**0.0463**	**0.0420**
$6_1^+ \to 4_1^+$	0.0406(27)[b]	>0.0246[c]			0.1941(563)[n]	
					0.1252(688)[l]	
					>0.0376[m]	
	0.1174	**0.1333**	**0.1382**	**0.1526**	**0.1601**	**0.1777**
$6_2^+ \to 4_1^+$		0.0010(1)[c]	>0.0001[g]			<0.0180[o]
	0.0088	**0.0103**	**0.0188**	**0.0068**	**0.0005**	**0.0010**
$6_2^+ \to 4_2^+$						<0.2469[o]
	0.0620	**0.0720**	**0.0788**	**0.0949**	**0.0935**	**0.0676**
$8_1^+ \to 6_1^+$	0.000017(2)[b]	0.0015(1)[c]	0.0018(7)[g]		0.0059(6)[m]	
	0.0008	**0.0013**	**0.0017**	**0.0017**	**0.0024**	**0.0020**
$8_2^+ \to 6_1^+$	0.0485(116)[b]	>0.0134[c]			0.2504(689)[k]	
					0.1722(563)[l]	
					>0.0626[m]	
	0.0923	**0.1190**	**0.1080**	**0.0379**	**0.0230**	**0.0024**
$8_2^+ \to 6_2^+$	<0.0396[b]	>0.0161[c]			0.0845(250)[k]	
					>0.0187[m]	
	0.0105	**0.0077**	**0.000036**	**0.0255**	**0.0286**	**0.0033**
$10_1^+ \to 8_1^+$	0.0059(20)[b]				0.0001(1)[l]	
					0.0001(31)[m]	
	0.0186	**0.0222**	**0.000011**	**0.000013**	**0.0001**	**0.1160**
$10_2^+ \to 8_1^+$	0.0156(3)[b]				0.2222($^{+407}_{-657}$)[k]	
					>0.0501[l]	
					>0.0028[m]	
	0.000	**0.000005**	**0.0230**	**0.0265**	**0.0027**	**0.0269**
$10_2^+ \to 8_2^+$	0.0263(6)[b]				0.2317(751)[m]	
	0.0659	**0.0036**	**0.0098**	**0.0010**	**0.0299**	**0.0007**
$12_1^+ \to 10_1^+$		0.0026(4)[c]		0.11(1)[i]	0.1283(63)[l]	
					0.1221(63)[m]	
	0.0527	**0.0002**	**0.1574**	**0.1570**	**0.1572**	**0.1562**
$12_2^+ \to 10_1^+$		0.0054(7)[c]			>0.0001[m]	
	0.000001	**0.0595**	**0.000025**	**0.0013**	**0.0006**	**0.0003**
$12_2^+ \to 10_2^+$					0.1158(63)[m]	
	0.0003	**0.000048**	**0.0658**	**0.0080**	**0.1643**	**0.1684**

TABLE III. (*Continued.*)

Transition	^{102}Cd	^{104}Cd	^{106}Cd	^{108}Cd	^{110}Cd	^{112}Cd
$14_1^+ \rightarrow 12_1^+$		0.0130(26)[c]		0.12(1)[i]	>0.0438[l]	
					0.0907(94)[m]	
	0.000006	**0.1616**	**0.1692**	**0.1704**	**0.1710**	**0.1721**

[a]From Ref. [6]; [b]From Ref. [5]; [c]From Ref. [7]; [d]From Ref. [46]; [e]From Ref. [47]; [f]From Ref. [9]; [g]From Ref. [39]; [h]From Ref. [40]; [i]From Ref. [8]; [j]From Ref. [48]; [k]From Ref. [41]; [l]From Ref. [11]; [m]From Ref. [10]; [n]From Ref. [13]; [o]From Ref. [12,42]; [p]From Ref. [49].

isotopes seem to be overestimated because the experimental excitation energies of some of these isotopes are tentative. The disagreement may also be due to the fact that the fixed value of deformation parameters is taken in the present calculations for the determination of the entire excitation spectra. The two excited 10_2^+ and 10_3^+ states in ^{104}Cd [Fig. 2(b)] at energies 4.329 and 4.466 MeV are well reproduced by the present calculations, and they are assigned to configurations 2-qp $(\nu h_{11/2})^2$ and 2-qp $(\pi g_{9/2})^2$, respectively. Similarly, excited states above 6^+ in ^{106,108}Cd [Figs. 2(c) and 2(d)] are reproduced within acceptable accuracy and assigned to configurations, presented in Tables I and II of the Supplemental Material [43]. In the case of ^{110,112}Cd [Figs. 2(e) and 2(f)], all the second excited states are reproduced well by the present calculation, and the assigned configurations are presented in Table II of the Supplemental Material [43]. The 6_3^+, 8_3^+, 10_3^+, 8_4^+, and 10_4^+ excited states are also seen to be reproduced well by the present calculations.

B. Electromagnetic quantities

The interpretation of electromagnetic quantities is the crucial test for the nuclear models. Therefore, the $E2$ transition probabilities and g factors are determined by using the PSM wave functions for the considered set of Cd isotopes. The formulas used for the calculation of $B(E2)$s and gyromagnetic factors (g factors) are the same as taken in early PSM works in Refs. [44,45]. In the following subsections the comparison of experimental and theoretical $B(E2)$ values and g factors is discussed.

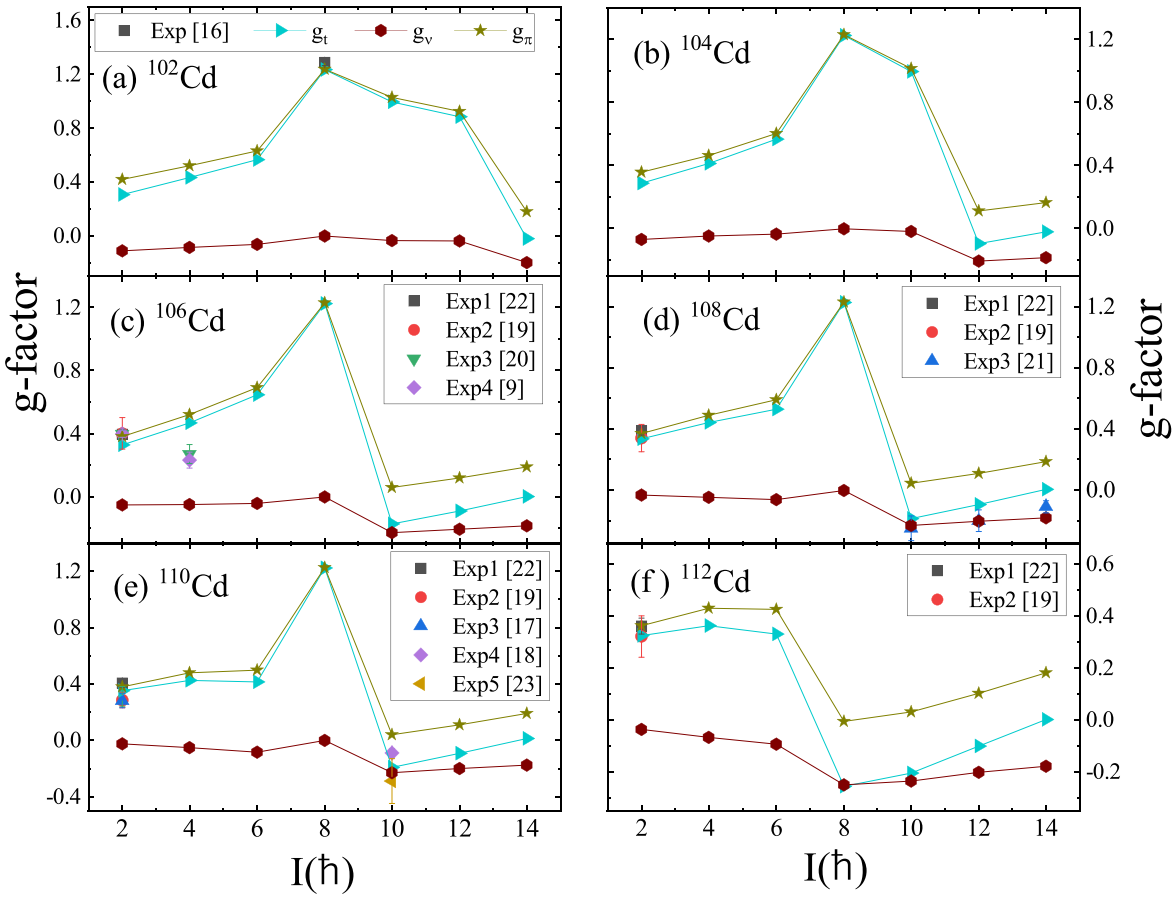

FIG. 3. Comparison of the theoretical total g-factors (g_t) with the available experimental data [9,16–23] and the contribution of proton (g_π) and neutron (g_ν) components to the total g-factor (g_t).

1. E2 transition probabilities

The theoretical $B(E2)$ values are compared with the experimental data [5–7,9–12,39–42,46–49] in Table III. The fixed value of effective charge $e_{\text{eff}} = 0.7$ is employed for the calculation of $B(E2)$ values of all the isotopes. The comparison presented in Table III shows that the experimental $B(E2)$ values of $2_1^+ \rightarrow 0_1^+$ and $4_1^+ \rightarrow 2_1^+$ transitions are well reproduced by the present calculations. The depletion in the $B(E2)$ values observed at the $8_1^+ \rightarrow 6_1^+$ transition in $^{102-106}$Cd is also well reproduced. The depletion in the $B(E2)$ values is due to the change in the structure of the yrast states around the spin $I = 6^+$. The $B(E2)$ value of the $4_1^+ \rightarrow 2_1^+$ transition in ^{110}Cd is exactly reproduced by the present calculations. The $B(E2)$ values of all other excited states are reproduced qualitatively.

2. g factors

The g factors provide the information about the character of the excited states and are rigorous tests for the nuclear models. From the magnetic moment measurements of $^{102-112}$Cd [9,16–23], it has been established that the yrast 8^+ states in the lighter Cd isotopes have $(\pi g_{9/2})^2$ character whereas the 10^+ yrast states in the medium-mass ones have $(\nu h_{11/2})^2$ character. Therefore, to investigate the nature of yrast states in the considered Cd isotopes, the g factors are computed by using PSM wave functions.

In the present calculations, the standard values taken for the gyromagnetic factor for orbital and spin angular momenta (g_l and g_s) are

$$g_l^\pi = 1, \quad g_s^\pi = 5.586\times 0.75,$$
$$g_l^\nu = 0, \quad g_s^\nu = -3.826\times 0.75.$$

The damping factor of 0.75 is used to damp g_l^π and g_s^ν from the free-nucleon values and for taking into account the core-polarization and meson-exchange current corrections [50].

Figure 3 compares the theoretical total g factors (g_t) with the available experimental data [9,16–23]. In the same figure, the contribution of proton (g_π) and neutron (g_ν) components to the total g factor (g_t) is also displayed. The available experimental data on g factors are reproduced well by the present calculations with the exception of $g(4_1^+)$ in ^{106}Cd. The 2^+ and 4^+ states are predicted to have small values of g factors due to the 0-qp configurations of these states where protons and neutrons are paired. The contribution to g_t is seen to be mainly from g_π up to spin $I = 10^+$ in ^{102,104}Cd and up to spin $I = 8^+$ in $^{106-110}$Cd. The peak observed in g_t at spin $I = 8^+$ in $^{102-110}$Cd is due to the alignment of a pair of protons in the $(\pi g_{9/2})^2$ orbital. The sudden dip in the g factors observed at spins $I = 14^+$, 12^+, 10^+, 10^+, 10^+, 8^+, respectively, in $^{102-112}$Cd is due to the contribution of neutrons to the g_t values, and it may be due to the alignment of neutrons in the $(\nu h_{11/2})^2$ orbital. The experimental observation [16] that the 8^+ state in light ^{102}Cd have $(\pi g_{9/2})^2$ character is supported by the present calculations. Besides, the experimental observation [18,21,23] that 10^+ states in medium-mass ^{108,110}Cd have $(\nu h_{11/2})^2$ character is also supported by the present calculations.

V. SUMMARY

Motivated by the recent remeasurement of spectroscopic quantities in $^{102-112}$Cd isotopes, the study of the ground and excited states of these isotopes is performed in relativistic and beyond mean-field approaches, respectively. The PESs of ground states of these isotopes are obtained by using the RHB model with the DD-ME2 interaction. The PESs establish the ground states of these isotopes as prolate moderately deformed. The β_2 extracted from the PESs of these isotopes are employed as input ϵ_2 in the PSM to study the structure of excited states. The resulting excitation spectra, $B(E2)$ values, and g factors are compared with the available experimental data. In all the considered Cd isotopes, the yrast energies up to $I = 4^+$ reproduces well the experimental data and arise from the pure 0-qp configuration. The theoretical yrast 6^+ and 8^+ states have 75% admixtures of the 2-qp $(\pi g_{9/2})^2$ configuration in addition to the 0-qp configuration in all the considered Cd isotopes. The configuration of the theoretical yrast 10^+ states in light ^{102,104}Cd is predicted to be 2-qp $(\pi g_{9/2})^2$ whereas the configuration of medium-mass $^{106-112}$Cd is predicted to be 2-qp $(\nu h_{11/2})^2$. The experimental excitation energies in ^{104}Cd have been revised by Muller *et al.* [7] which are well reproduced by the present calculations. The experimental excited states of some Cd isotopes are reproduced satisfactorily, and their configurations are predicted. The experimental $B(E2)$ values of $2_1^+ \rightarrow 0_1^+$ and $4_1^+ \rightarrow 2_1^+$ transitions are well reproduced by the present calculations. The depletion in the $B(E2)$ values observed at the $8_1^+ \rightarrow 6_1^+$ transition in $^{102-106}$Cd is also well reproduced.

The depletion in the $B(E2)$ values is due to the change in the structure of the yrast states around the spin $I = 6^+$. The available experimental data on g factors are reproduced well by the present calculations with the exception of $g(4_1^+)$ in ^{106}Cd. The sudden dip in the g factors observed at spins $I = 14^+$, 12^+, 10^+, 10^+, 10^+, 8^+, respectively, in $^{102-112}$Cd is due to the contribution of neutrons to the g_t values, and it may be due to the alignment of neutrons in the $(\nu h_{11/2})^2$ orbital. The experimental observations [16,18,21,23] that the 8^+ states in light ^{102}Cd have $(\pi g_{9/2})^2$ character and the 10^+ states in medium-mass ^{108,110}Cd have $(\nu h_{11/2})^2$ character are well supported by the present calculations.

ACKNOWLEDGMENTS

The computations in this paper were supported by the SAMKHYA: High performance Computing Facility provided by the Institute of Physics, Bhubaneshwar. We are thankful to Professor S. K. Patra, Professor Y. Sun, and Professor J. A. Sheikh for their collaborations. One of the authors, S.S. acknowledges the Council of Scientific and Industrial Research, New Delhi for providing Senior Research Fellowship Vide File No. 09/100(0227)/2019-EMR-1.

[1] G. de Angelis *et al.*, Phys. Rev. C **60**, 014313 (1999).
[2] J. Kumpulainen, R. Julin, J. Kantele, A. Passoja, W. H. Trzaska, E. Verho, J. Vaaramaki, D. Cutoiu, and M. Ivascu, Phys. Rev. C **45**, 640 (1992).
[3] S. Juutinen *et al.*, Nucl. Phys. A **573**, 306 (1994).
[4] F. Corminboeuf, T. B. Brown, L. Genilloud, C. D. Hannant, J. Jolie, J. Kern, N. Warr, and S. W. Yates, Phys. Rev. C **63**, 014305 (2000).
[5] K. P. Lieb *et al.*, Phys. Rev. C **63**, 054304 (2001).
[6] N. Boelaert, A. Dewald, C. Fransen, J. Jolie, A. Linnemann, B. Melon, O. Moller, N. Smirnova, and K. Heyde, Phys. Rev. C **75**, 054311 (2007).
[7] G. A. Muller *et al.*, Phys. Rev. C **64**, 014305 (2001).
[8] A. J. Simons *et al.*, Phys. Rev. C **72**, 024318 (2005).
[9] N. Benczer-Koller *et al.*, Phys. Rev. C **94**, 034303 (2016).
[10] M. Piiparinen *et al.*, Nucl. Phys. A **565**, 671 (1993).
[11] S. Harissopulos, A. Dewald, A. Gelberg, K. O. Zell, P. von Brentano, and J. Kern, Nucl. Phys. A**683**, 157 (2001).
[12] P. E. Garrett, K. L. Green, H. Lehmann, J. Jolie, C. A. McGrath, M. Yeh, and S. W. Yates, Phys. Rev. C **75**, 054310 (2007).
[13] P. E. Garrett *et al.*, Phys. Rev. C **86**, 044304 (2012).
[14] P. E. Garrett *et al.*, Phys. Rev. Lett. **123**, 142502 (2019).
[15] P. E. Garrett *et al.*, Phys. Rev. C **101**, 044302 (2020).
[16] D. Alber *et al.*, Z. Phys. A: At. Nucl. **344**, 1 (1992).
[17] G. W. Wang, A. J. Becker, L. M. Chirovsky, J. L. Groves, and C. S. Wu, Phys. Rev. C **18**, 476 (1978).
[18] P. H. Regan, A. E. Stuchbery, and S. S. Anderssen, Nucl. Phys. A **591**, 533 (1995).
[19] J. M. Brennan, M. Hass, N. K. B. Shu, and N. Benczer-Koller, Phys. Rev. C **21**, 574 (1980).
[20] G. J. Kumbartzki *et al.*, Phys. Rev. C **93**, 044316 (2016).
[21] P. Fan *et al.*, Hyperfine Interact. **230**, 155 (2015).
[22] S. K. Chamoli *et al.*, Phys. Rev. C **83**, 054318 (2011).
[23] T. J. Gray *et al.*, Phys. Rev. C **96**, 054332 (2017).
[24] T. Schmidt, K. L. G. Heyde, A. Blazhev, and J. Jolie, Phys. Rev. C **96**, 014302 (2017) and references therein.
[25] P. Kumar and S. K. Dhiman, Mod. Phys. Lett. A **35**, 2050189 (2020).
[26] K. Nomura and J. Jolie, Phys. Rev. C **98**, 024303 (2018) and references therein.
[27] L. Prochniak, P. Quentin, and M. Imadalou, Int. J. Mod. Phys. E **21**, 1250036 (2012).
[28] P. Fleischer, P. Klupfel, P.-G. Reinhard, and J. A. Maruhn, Phys. Rev. C **70**, 054321 (2004).
[29] B. Maheshwari, H. A. Kassim, N. Yusof, and A. K. Jain, Nucl. Phys. A **992**, 121619 (2019).
[30] T. Niksic, P. Ring, D. Vretenar, Y. Tian, and Z.-Y. Ma, Phys. Rev. C **81**, 054318 (2010).
[31] T. Niksic, N. Paar, D. Vretenar, and P. Ring, Comput. Phys. Commun. **185**, 1808 (2014).
[32] G. A. Lalazissis, T. Niksic, D. Vretenar, and P. Ring, Phys. Rev. C **71**, 024312 (2005).
[33] Y. Tian, Z.-Y. Ma, and P. Ring, Phys. Rev. C **79**, 064301 (2009).
[34] K. Hara and Y. Sun, Int. J. Mod. Phys. E **4**, 637 (1995).
[35] Y. Sun and K. Hara, Comput. Phys. Commun. **104**, 245 (1997).
[36] Y. Sun, Phys. Scr. **91**, 043005 (2016).
[37] T. Bengtsson and I. Ragnarsson, Nucl. Phys. A **436**, 14 (1985).
[38] P. Ring and P. Schuck, *The Nuclear Many-Body Problem* (Springer, Berlin, 1980).
[39] D. De Frenne and A. Negret, Nucl. Data Sheets **109**, 943 (2008).
[40] J. Blachot, Nucl. Data Sheets **91**, 135 (2000).
[41] G. Gurdal and F. G. Kondev, Nucl. Data Sheets **113**, 1315 (2012).
[42] S. Lalakovski and F. G. Kondev, Nucl. Data Sheets **124**, 157 (2015).
[43] See Supplemental Material at http://link.aps.org/supplemental/10.1103/PhysRevC.103.064312 for the detailed quasiparticle configurations of the yrast and excited states for even-even $^{102-112}$Cd.
[44] Y. Sun and J. L. Egido, Nucl. Phys. A **580**, 1 (1994).
[45] Y. Sun and J. L. Egido, Phys. Rev. C **50**, 1893 (1994).
[46] W. T. Milner, F. K. McGowan, P. H. Stelson, R. L. Robinson, and R. O. Sayer, Nucl. Phys. A **129**, 687 (1969).
[47] M. T. Esat, D. C. Kean, R. H. Spear, and A. M. Baxter, Nucl. Phys. A **274**, 237 (1976).
[48] J. Wesseling, C. W. De Jager, J. B. van der Laan, H. de Vries, and M. N. Harakeh, Nucl. Phys. A **535**, 285 (1991).
[49] D. De Frenne and E. Jacobs, Nucl. Data Sheets **79**, 639 (1996).
[50] B. Castel and I. S. Towner, *Modern Theories of Nuclear Moments* (Clarendon Press, Oxford, 1990).